Simulation and Modeling of the *Rhodobacter sphaeroides* Bacterial Reaction Center: Structure and Interactions

Matteo Ceccarelli[†]

CECAM, Centre Européen de Calcul Atomique et Moleculaire, Ecole Normale Superieure de Lyon, 46 Allée d'Italie, 69364 Lyon, France

Massimo Marchi*

Commissariat à l'Energie Atomique, DSV-DBJC-SBFM, Centre d'Études, Saclay, 91191 Gif-sur-Yvette Cedex, France

Received: September 16, 2002; In Final Form: November 22, 2002

In this paper, we present the structural and dynamic results of a 3.4 ns molecular dynamics simulation of a reaction center protein immersed in a micelle-like environment formed by a detergent, lauryl dimethyl amino oxide or LDAO, and hydrated by more than 6000 additional water molecules. The whole system, ≈40 000 atoms, was simulated using an all-atom force field with refined potential parameters developed by us to describe the protein cofactors and the detergent molecules. LDAO, inserted at the beginning of the run in a configuration far from equilibrium, rearranged forming a micelle attached to the hydrophobic regions of the protein. The micelle is a stable and dynamic structure over the whole trajectory and prevents the protein and the internal cofactors from contacts with water. Comparing our simulated system with the high-resolution crystallographic structure, the deviations of the backbone atoms are small, less than 1.8 Å after 3.4 ns, and the chromophore arrangement geometry is stable and close to X-ray for the whole simulation. Thus, our system constitutes a realistic model to investigate at an atomic level the role of the protein environment on the charge transfer processes taking place in this complex. Related to the functionality of this RC protein, we observe the isomerization of the tyr M210 which is directly coupled with the primary electron transfer. Concerning the branch functionality of the RC, we observe that the computed minimum distance between the chromophores on the L and M side has a different dynamic behavior and is smaller on average for transitions on the L side. This finding might have some bearing on the electron-transfer asymmetry of the primary charge transfer.

I. Introduction

Membrane proteins play a crucial role in cellular recognition. Because of their role in the exchange of matter (electrons, protons, ions, etc.) between the two sides of cellular membranes, they are perforce composed of hydrophobic and hydrophilic regions. Although the former regions are in direct contact with the phospholipid membrane or other membrane proteins, the latter allow for exchanges with the solvent. The amphiphilic nature of membrane proteins and their large size make molecular modeling more arduous than for simpler globular proteins. In particular, it requires the introduction of hydrophobic interactions to mimic the effect of the membrane on the protein. This can be done either using explicit models of membrane or a membrane-mimetic system such as octane.[1] Although the former is more realistic, the large dimension and the long times needed to relax the system[2] limited in the past their applications. On the other hand, the use of a model system is easier to treat and useful when protein properties do not depend on the specific lipid composition.[3]

We focus here on the molecular modeling and simulation of the reaction center protein (RC) involved in bacterial photosynthesis. In purple bacteria, RC is involved in the first step of the photosynthesis which involves the transformation of light energy into chemical energy. The protein is composed of three principal subunits, called L, M, and H, with the first two sharing a 2-fold axis of quasisymmetry. The L and M proteins bind in their interior several cofactors arranged as in Figure 1 and having the same symmetry axis (from P to the non-heme iron). These cofactors, 4 bacteriochlorophylls (B), 2 bacteriopheophytins (H), 2 ubiquinones (Q), and one iron ion, are directly involved in the initial step of the photosynthesis: After photoexcitation of the bacteriochlorophyll dimer, called the special pair (P), the excited electron moves first to the bacteriopheophytin of the L side (H_L) covering 17 Å in 3 ps,[4,5] then to the quinone molecule (Q_A) close to the and finally to a second quinone (Q_B).

Because the three-dimensional structure of the of two purple bacteria has been resolved by X-ray crystallography,[6,7] only a few molecular dynamics (MD) simulations have been carried out. In earlier times, simulations were carried out by simply restricting the simulation only to regions close to the chromophores involved in the electron transfer,[8−10] while the remaining protein was kept frozen in its X-ray conformation. Parson and co-workers improved upon this by representing the solvent and the membrane effects on the dynamics and electron transfer through a dielectric model based on Langevin dipoles (see ref 11 and references therein). In a previous paper[12] focused

* To whom correspondence should be addressed. E-mail: marchi@villon.saclay.cea.fr.

† Present address: CSCS/ETHZ, Via Cantonale, CH-6928 Manno, Switzerland. E-mail: mcecca@cscs.ch.

10.1021/jp0270001 CCC: $25.00
Published on Web 01/21/2003

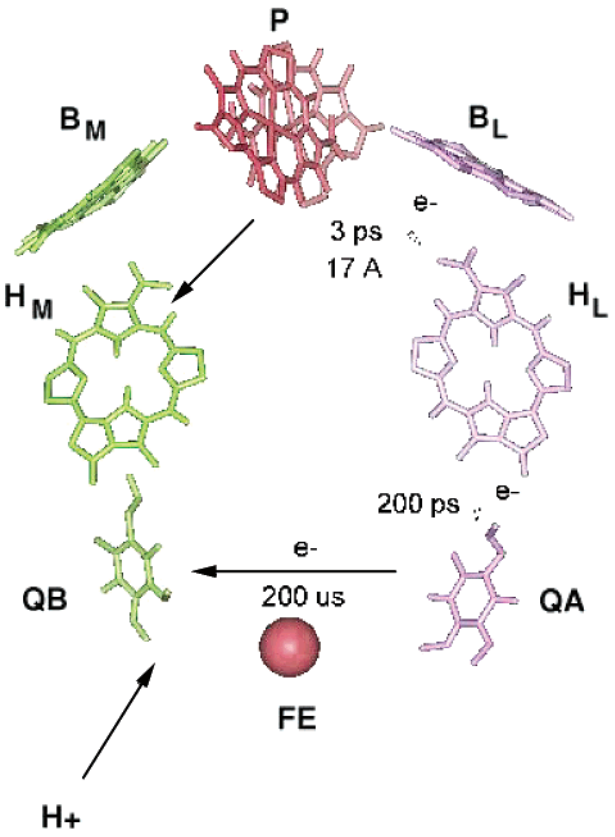

Figure 1. Arrangement of the cofactors in the photosynthetic reaction center of *Rb. sphaeroides*. Arrows show the electron and proton-transfer pathways.

on the dynamics of the special pair excited state, we simulated the reaction center of *Rhodobacter* (*Rb.*) *sphaeroides* in water without modeling the hydrophobic interactions of the membrane. Not surprisingly, the largest deviation from X-ray crystallography was found for the transmembrane helices.

The present investigation reports on a new molecular modeling of the RC protein of *Rb. sphaeroides*. Given the recent improvements in MD algorithms and the ever increasing power of modern computers, we have been able to simulate a protein in an amphiphilic environment. In particular, detergent molecules (lauryl dimethyl amino oxide, or LDAO, used experimentally to solubilize RC's) are used to protect the transmembrane helices, whereas water solvates the RC hydrophilic regions and the detergent headgroups. Indeed, low resolution neutron diffraction experiments showed that the detergent plays a decisive role in the crystallization.[13] After eliminating lipid molecules by aggregation, it facilitates the ordered packing of the protein by binding to their hydrophobic surfaces in micellar manner. Because the presence of the detergent on the protein surface does not alter its structure and functionality, such a molecular complex provides a good model to investigate electron and proton transfer in RC's proteins.

In our system, LDAO replaces in a natural way the phospholipid membrane environment surrounding the RC in bacteria and keeps the system size manageable by present days molecular modeling. The long trajectory sampled by our simulation, 3.4 ns, enables us to sufficiently relax and equilibrate the detergent. Much longer simulations would have been needed if phospholipids were used instead of LDAO.

Thus, our all-atom MD simulation enables for the first time the investigation of electron and proton transfer in a RC protein in a realistic environment with accurate electrostatic interactions and without geometrical constraints. This first paper is focused on the structural properties and stability of a photosynthetic RC protein in this micelle-like environment. The atomic-level analysis of this simulation, reported here, provides detailed information on the behavior of the detergent complex and its interaction with the protein and the water molecules. It also sheds light on the structural changes affecting the primary charge separation. In a forthcoming paper, we report results on the kinetics of the primary electron transfer.[14]

The paper is organized as follows: In section II, we give details of the simulation and discuss the microscopic model and the simulation set up and runs. The structural and dynamic results of our MD runs are analyzed in section III. The paper ends with a conclusion.

II. Simulation Details

A. Microscopic Model. As the initial atomic coordinates of the RC protein from *Rb. sphaeroides* we used the high resolution ($R = 2.65$ Å) structure due to Ermler et al.,[15] Protein Data Bank entry 1pcr. This includes the coordinates of the three principal RC subunits, 9 cofactors, 160 crystallization waters, 9 lauryldimethyl amino oxide, LDAO, detergent molecules, and one carotenoid molecule attached at the M subunit.

The latter molecules, which protects RC's against photooxidation by quenching the triplet state of P, was not considered in our molecular modeling. Indeed, the main interest of our investigation is the primary charge separation, and RC's are known to sustain electron transfer also in their carotenoid depleted form (see, for example, experimental data on the R26 mutant[16]).

In the high-resolution X-ray structure by Ermler et al. only a few tightly bound LDAO molecules were detected. However, a lower resolution neutron scattering study of the RC crystal[13] showed that the detergent is concentrated and covers the transmembrane regions of the RC protein, about 25−30 Å in length along the C_2 quasisymmetry axis. Indeed, in the crystal, and probably in solution, LDAO is arranged as a micelle-like structure around the RC, protecting from water its eleven transmembrane helices. Thus, to reproduce the hydrophobic environment around the RC, our modeling included 150 additional LDAO molecules in the proximity of the RC's transmembrane helices. We notice that, in this way, the total number of LDAO, 159, is consistent with biochemical analysis performed on bacteriorhodopsin[17] which has dimensions of the protein hydrophobic core comparable with those of RC's. The next section will describe in detail how these extra LDAO molecules were added.

The solvent interacting with the RC protein was simulated explicitly. Even though explicit models of water are computationally more expensive than continuum or other approximate electrostatic theories, they make no mesoscopic approximation in handling the water−protein interactions. Especially at short range where hydrogen bonds and steric effects are dominant, they are far superior than implicit techniques.[18,19]

An all-atom force field was used to simulate our solvated RC. Although for the protein and water the AMBER force field and the TIP3P model were used, respectively, all of the cofactors of RC and LDAO were parametrized by us. Our force field development was carried out consistently with the AMBER force fields and made use of both DFT calculations and crystallographic data.[20,21] ESP (electrostatic potential fit) charges and intramolecular force constants were obtained directly from ab initio results and then tested against data in condensed phase.

Concerning the RC's chromophores, simulations were carried out only in their ground electronic state as determined by DFT. The protonated state of all of the amino acids were those at pH = 7, assuming standard pK_a values except for glutamate L104, as in a previous simulation,[12] which was protonated, according to X-ray findings. Simulations were performed with the parallel version of the program ORAC.[22−24] A smooth treatment of long-range electrostatic contributions[25,26] in conjunction with external constraints[27] for pressure and temperature allowed us to simulate our system with the most realistic conditions possible with today's computational technology.

B. Preparation of the System. As a first step in the modeling of the RC protein, hydrogens coordinates, not known experimentally, were added by geometric rules to the X-ray coordinates. Subsequently, to relieve structural stress in the assembly, the coordinates of the RC protein in vacuo were minimized by a few MD steps (5 ps in total) at 20 K. At this stage, deviations from the X-ray structure were less than 0.5 Å.

Because the coordinates of all of the detergent bound to the protein surface are not available from X-ray, the second step of our RC modeling was to place the LDAO. First, the RC protein was rotated and translated to have its center of mass and its C_2 quasisymmetry axis coincident with the origin and the Z axis, respectively. Second, five planes normal to the Z axis and at a distance of 6.5 Å from each other were generated to cover the transmembrane region of the protein along Z, i.e., approximately 25−30 Å. On each plane, we disposed at regularly spaced angles 30 LDAO molecules in their all-trans conformation, tail at the intersection of the Z axis with the plane and head pointing toward the exterior. Third, each LDAO was translated along their molecular axis toward the exterior of the protein so as to reach 3 Å between the nearest protein surface atom and each detergent tail. Equilibration of the LDAO molecules were performed by MD in a vacuum at 250 K for 30 ps and at 400 K for 230 ps. During these simulations, the protein atoms were not allowed to move. Because our starting point was a conformation of the LDAO molecules far from equilibrium, a rather long relaxation time was needed to move LDAO away from the all-trans molecular configurations and to allow a new rearrangement around the protein. Indeed, in a few hundred picoseconds at 400 K, a temperature well above the melting point (340 K), the detergent molecules formed a compact micelle-like structure around the protein. At the same time the configurational energy of the complex decreased considerably.

Finally, the system LDAO + RC was hydrated in an orthorhombic box of dimensions 76 × 84 × 80 Å containing TIP3P water at standard density. With this choice, each protein or detergent surface atom had at least two water shells before the box edges. The system contained in the end 6323 water molecules, 159 (9 molecules were crystallographic) and one protein complex, for a total of 40 327 atoms.

Following this initial preparation phase, standard constant pressure−temperature MD was started. In all simulations, short-range nonbonded interactions were calculated up to a 10 Å cutoff, whereas long-range electrostatic interactions were treated by the SPME method[26] using a very fine grid, 128 point per axis, with periodic boundary conditions, and Ewald convergence parameter α of 0.43 Å^{-1}. Three different Nosé−Hoover thermostats[28] were coupled to solute, solvent, and total center of mass.[24] An external pressure of 0.1 MPa was applied all along the trajectory. A five time-step rRESPA[29] algorithm with times of 0.5−1.0−2.0−4.0−12.0 fs was used with bond constraints on hydrogen covalent bonds handled by a Shake-Rattle-like algorithm.[30,31] The combination of the above integration techniques, already tested in the past on similar systems,[24] ensures both good accuracy in energy conservation and a large CPU saving for simulation in the NPT ensemble.

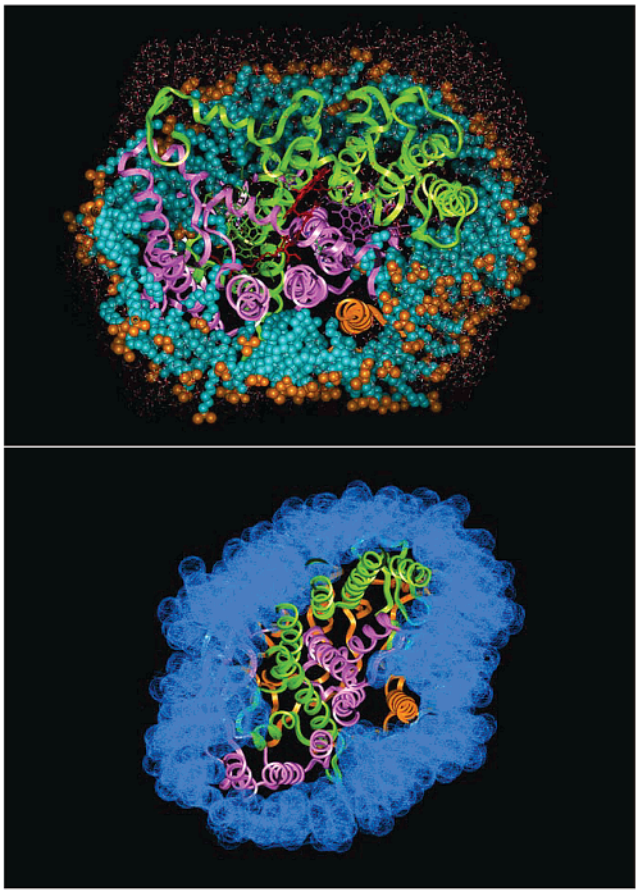

Figure 2. Pictorial representation of the simulated system after 3.4 ns. On the top panel, an instantaneous picture of the simulation box; on the bottom, a view of the RC protein helices embedded in an average representation of the detergent micelle. The plane of the pictures is normal to the C_2 quasisymmetry axis of the RC protein.

The final system was first equilibrated with velocity rescaling for 15 ps at 50 K and 80 ps at 300 K. Following this initial equilibration, we ran the system for one additional nanosecond at constant temperature (T = 300 K) and pressure (P = 0.1 MPa). To achieve full relaxation, the simulation box was entirely flexible[32] for the first 300 ps, whereas for the remainder of the run, only isotropic changes of the box were allowed.[24] Finally, the system was simulated for an additional 2.4 ns. Atomic coordinates were saved every 250 fs for a total of 9600 configurations. The 3.4 ns run took 19 CPU days on 32 processor on the parallel Cray T3E of CEA-Grenoble and IDRIS-Orsay.

III. Results and Discussion

A. Simulation Box. During a first phase of simulation with a fully flexible cell, the system box changed its shape to arrive after 300 ps to an almost hexagonal primitive cell with angles between cell axis, α, β, and γ of 81.6, 81.3, and 69.4°, respectively. Afterward, the MD simulation continued with a barostat allowing only isotropic fluctuations of the cell volume.[24] The averaged cell parameters computed from the 2.4 ns long acquisition trajectory are a = 67.9, b = 82.5, and c = 74.9 Å, for an average volume of 386 231 Å^3. This compares to an initial value of 510 720 Å^3. Figure 2 displaying a typical view of the

simulation box after 3.4 ns shows the hexagonal symmetry of the simulated system.

B. Detergent. The lack of structural details on the bulk of the detergent molecules around the RC protein obtained from X-ray crystallography reflects the dynamic character of these aggregates. Low resolution neutron scattering experiments[13] on a crystal of a RC protein (*Blastochloris* (*Bl.*), formerly called *Rhodopseudomonas*, *Viridis*) have shown that detergent forms micellar structures around the protein hydrophobic regions. The computed LDAO envelop, displayed on the bottom panel of Figure 2 and averaged over the simulation time is very evocative of the experimental neutron scattering results.

Our MD simulation offers also the possibility to analyze in detail the detergent behavior at the atomic level. It also makes it possible to investigate the nature of the protein−membrane interaction and the role of the lipid environment on the peptide conformational properties.

In the following, we report a quantitative analysis of the detergent to investigate whether a stable detergent structure exists. This step is necessary as this is, to our knowledge, the first simulation of a protein−detergent complex. We then analyze the molecular behavior and the interaction with the protein and with water.

1. Structure and Dynamics. The detergent stability was analyzed by calculating, for the last 2.4 ns of the trajectory, the center of mass position (COM) with respect to the protein center of mass and the three principal moments of inertia (MOI) of the LDAO aggregate. The former gives information on its position relative to the RC, whereas the latter provides clues on its shape. Although in our case the detergent does not have a spherical or ellipsoidal shape as those found in true micelles in solution, the behavior of MOI provides information on its shape. We first find that fluctuations of a few tenth of angstrom and with large time scales (hundreds of picoseconds) are present in each of the COM components. In particular, the *X* and *Y* values fluctuate around mean values in an almost anticorrelated fashion. On the other hand, the *Z* component shows a small drift (less than 1 Å within 2.4 ns), indicating that the detergent undergoes a translation to go away from the H subunit, reaching a more suitable position relative to the RC complex.

Next, we analyzed the dynamical properties of the protein and LDAO by computing the self-diffusion coefficient via the mean square displacement:

$$\langle r^2(t)\rangle = \frac{1}{N}\sum_{i=1}^{N}|r_i(t) - r_i(0)|^2 \qquad (1)$$

as a function of time. According to the Einstein relationship, the diffusion constant can be obtained by taking the limiting value of the slope:

$$D = \lim_{t\to\infty} \frac{\langle r^2(t)\rangle}{6\,t}$$

The mean square displacement for LDAO used to obtain *D* was computed including contributions only from the nitrogen heads. In this way, we monitor only the lateral diffusion of the detergent within the micelle-like structure, for the whole simulation the LDAO headgroups are found in contact with hydration water.

The diffusion coefficients computed for LDAO, water and protein, are shown in Table 1. Accordingly, the detergent forms a rather dynamic structure compared to the protein atoms, having a 13 times larger diffusion, *D*. The value of *D* found for the detergent is typical of a system in the gel phase.[33] Water shows the largest diffusion constant close to that for experimental bulk water. Because bulk TIP3P water diffuses twice as fast as experiment, this result indicates that simulation water is retarded by the protein.

TABLE 1: Self-Diffusion Constants, *D* [$m^2\ s^{-1}$], for the Different Components of the System, Protein, Detergent, and Water[a]

system	*D*
protein	$0.4\ 10^{-11}$
LDAO	5.3×10^{-11}
water	2.5×10^{-9}
water cryst.	1.4×10^{-9}
water expt.	2.3×10^{-9}

[a] For water, we compared the diffusion of all water and crystallographic water alone to the experimental value, last line.

TABLE 2: Probability to Find a Dihedral Angle of the Detergent Tails (C−C−C−C) in the Gauche Conformation[a]

dihedral no.	prob. gauche	dihedral no.	prob. gauche
1	0.43	6	0.50
2	0.43	7	0.43
3	0.48	8	0.47
4	0.44	9	0.44
5	0.47		

[a] Dihedrals are numbered starting from the first carbon in the tail.

The inspection of the three principal MOI as a function of the trajectory time reveals that, despite lateral diffusion and a some drift along the *Z* direction, the detergent maintains a regular shape during the 2.4 ns trajectory (data not shown).

The LDAO is a nonionic detergent molecule with a polar head formed by a nitrogen, binding two methyl groups, and an oxygen, and a hydrophobic tail formed by twelve saturated carbon atoms, C1 being the first and C12 the last carbon. Structural aspects of this aliphatic tail were first analyzed in terms of the populations of the trans and gauche conformers and of the C1−C12 distance. The probabilities to find a dihedral of the tail in the gauche conformation are in the range 0.43−0.50; see Table 2. These values are larger than in a previous study on spherical micelles[34] and are probably due to differences in the force field. In contrast with spherical micelles where steric constraints for tail carbons are important, the gauche probability for the tail carbons of our system is similar to that of the remaining carbons of the chain. This behavior makes the interior of our LDAO aggregate more similar to that of lipid bilayer than to the inside of a micelle.[35]

In Figure 3, we present the probability distribution for the C1−C12 distance. This shows an intense peak between 12.3 and 13.3 Å and a smaller one at 13.7 Å, this should be compared with a length for the all-trans LDAO of 14.2 Å. This behavior can be interpreted as being due to the lack of much steric constraints in the tail, so that a large number of molecules can stay near their extended configurations at the same time.

The orientation of the C1−C12 vector with respect to the *Z* axis and the *XZ* plane allows the characterization of the LDAO orientation around the protein complex. In the initial phase, the molecular axes of all of the LDAO molecules were oriented at 90° relative to the *z* direction. After the initial relaxation, we obtained a symmetrical distribution spread around this starting value. In Figure 4, we show the simulation averaged probability distribution of the C1−C12 orientation relative to the *z* axis (θ_z) and the *XZ* plane (θ_{xz}).

The probability of θ_z grows uniformly between 0° and 50°, and then from 50° to 130°, it is constant, to decrease afterward.

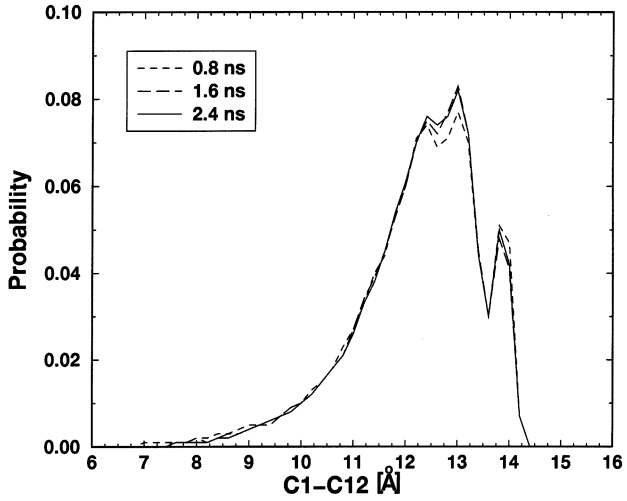

Figure 3. Probability distribution of the C1−C12 distance.

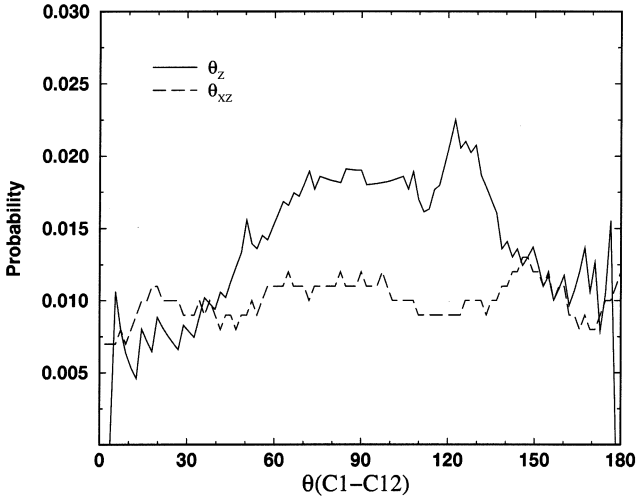

Figure 4. Probability distribution of the C1−C12 orientation relative to the *Z* axis (θ_z) and *XZ* plane (θ_{xz}).

Although preferential values for θ_z are at around 90°, a few molecules parallel to the *z* axis are also found. In contrast, θ_{xz} is constant all around the angular spectrum indicating that the detergent molecules are distributed regularly all around the protein on the *XZ* plane.

2. Interaction with the Protein and Water. For each carbon atom in the tails and for the nitrogen atoms of the heads, we have calculated the minimum distance from the protein surface. For all carbon atoms, the corresponding probability distribution (data not shown) presents two peaks: one more pronounced at 3.7 Å, indicating a strong interaction with the protein, and a broader peak at 7−8 Å, signaling a weaker bond. This result shows how contacts with the protein are possible not only for the last carbons in the tail but also for the remaining carbons. For the nitrogen bonded to two methyl groups, only one peak is found at 4.1 Å, because of the geometric hindrance of its ligand.

A first analysis of the detergent−water interaction was performed by calculating the hydration number, or N_w. This is defined as the average number of water molecules that stay in contact with each detergent atom; all detergent−water distances ≤3.5 Å are taken as a contact. N_w's were calculated for all of the carbon atoms in the hydrocarbon tails and for the nitrogen of the head. In Figure 5, we present the result for the carbon atoms of the chain. We notice that the hydration number is

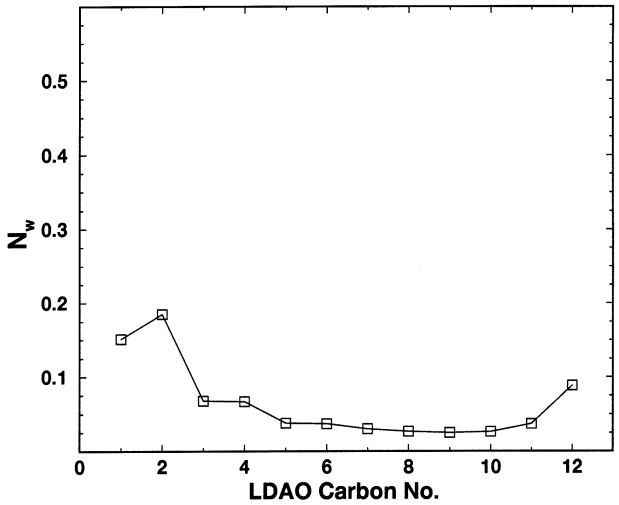

Figure 5. Hydration number as a function of the tail carbon atom in LDAO. Carbon atoms are labeled from C1 to C12.

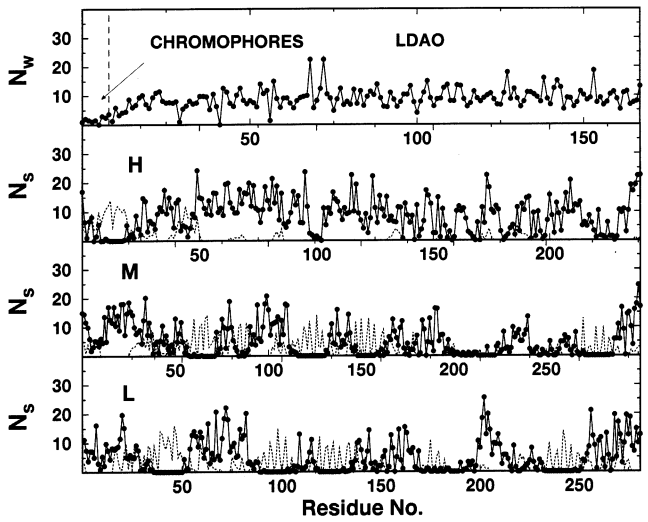

Figure 6. Solvation number, or N_s, for detergent, protein, and chromophores. For the RC protein, the hydration number (solid line) and the number of detergent molecules (dotted lines) are plotted. For the chromophores and LDAO the hydration number, or N_w, is presented (solid line).

smaller than 1 for all carbons, and it is smaller than 0.1 for carbons from C3 to C13. It is not surprising that hydration of C2 is higher than of C1, as the dimension of the headgroup prevents the contacts with C1. Overall, our findings for chain atoms agree well with simulations of isolated micelle.[34] For the hydrophilic head in contact with water, a hydration number of 6.9 is found.

Our findings on LDAO hydration give already strong indications that the presence of the detergent protects the 11 trans-membrane helices of the protein from water. This is confirmed in Figure 6 where we plot the solvation numbers, or N_s, as a function of the residue number. Here, we consider as solvent molecules both water and LDAO. In this case, a solvent molecule is considered in contact with a residue if any of their respective atoms are in Lennard-Jones contact with one another. Protein amino acids, detergent molecules, and cofactors are numbered as residues in Figure 6. We notice that the hydration number of the 11 trans-membrane regions is zero. At the same time, the number of detergent molecules in contact with the protein residues (dotted line in Figure 6) shows that the LDAO has a greater disposition to be located near the same trans-

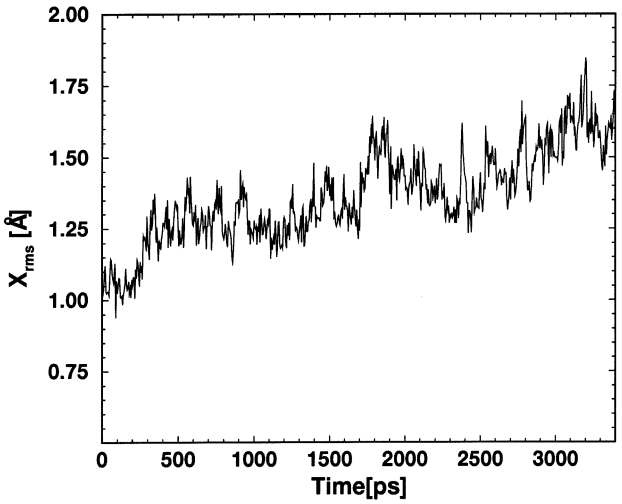

Figure 7. Instantaneous mean square deviation of the simulated RC protein from its X-ray structure as a function of simulation time. See text for further explanations.

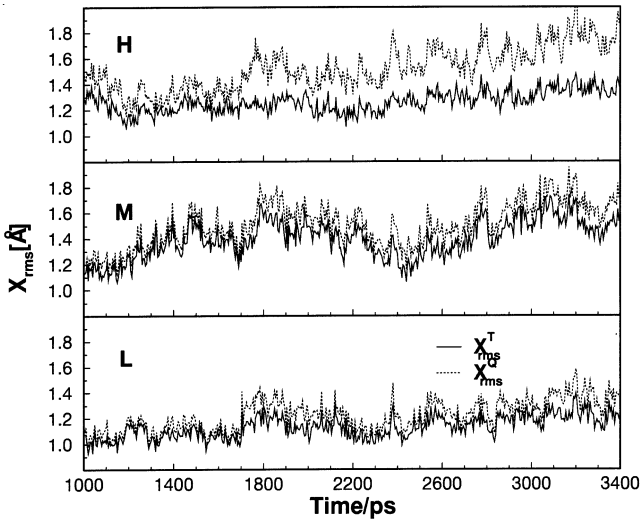

Figure 8. $X^{T}_{rms}$and X^{Q}_{rms} for the three RC protein subunits as a function of simulation time. See text for explanation.

membrane helices. Only two of these helices, located in the interior of the RC, are in contact with neither LDAO nor water molecules.

C. Protein Structure. During the simulation, the evolution of the protein structure was monitored by calculating the instantaneous mean square deviation of the backbone atoms from their X-ray structure or X_{rms}. Instantaneous here implies that no averages on the RC structure generated during the trajectory were carried out. The deviation is computed after performing a rigid body fit, only rigid rotations and translations are allowed, of the two structures to minimize the deviation. In Figure 7, we present the global instantaneous deviations of the entire protein. We notice that this value is not constant in time, showing sudden jumps after regions of almost constant deviations. In the initial segment of the trajectory up until 300 ps, which allowed for anisotropic cell fluctuations, X_{rms} is small, less than 1.0 Å, whereas the dimensions and shape of the cell vary substantially.

To investigate further the protein behavior, we calculated the X_{rms} of each of the ensemble of the three subunits, L, M, and H. Two quantities were computed for each subunit: X^{T}_{rms} is the X_{rms} obtained after a rigid body fit carried out only on the atoms of that subunit and X^{Q}_{rms} is instead the X_{rms} obtained by performing a rigid body fit of the ensemble. The former provides indications on the subunit tertiary structure, whereas the latter is a measure of the overall deviation of the subunit from its X-ray quaternary structure. The X^{T}_{rms}'s in Figure 8 show that the three subunits keep their tertiary structures close to their mean values. The L side in particular is the region closest to its crystal structure with a deviation near 1.2 Å. On the other hand, the M and H sides have larger deviations, near 1.4 Å, with more pronounced fluctuations for the M side.

Both subunits L and M have a stable X^{Q}_{rms} all along the trajectory. Also, the distances of their centers of mass from the axis center do not change much (not shown). On the contrary, the H side has a larger X^{Q}_{rms} which drifts to higher values during the simulation. We find that this drift is due to a translation of the H subunit center of mass from the center of the simulation box. At the same time, a similar drift along the *Z* axis is found for the center of mass detergent micelle-like structure.

A comparison of the crystallographic *B* factors with root mean square (RMS) fluctuations during the simulation is presented

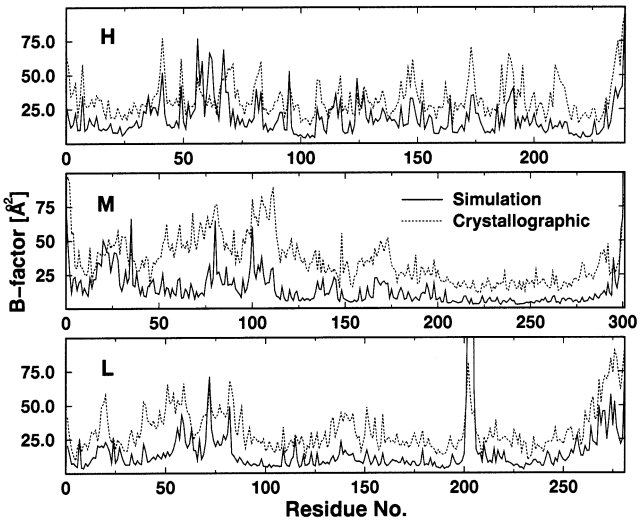

Figure 9. Experimental and simulated *B* factors for the three RC protein subunits.

in Figure 9 for each residue. Although the MD data are shifted down with respect to experiment, they may lack the contribution of the static lattice disorder, MD and X-ray maxima and minima are very well correlated with one another.

D. Structural Changes Affecting the Primary Charge Separation. The structural behavior of the chromophores and of the protein regions nearby affects directly the electron-transfer properties of the system. In a forthcoming paper,[14] we use a linear response theory to compute the free energy surfaces for the primary charge separation; here, we investigate changes in the local structure of the cofactors and focus on the formation and breaking of a hydrogen bond between tyr M210 and the P.

1. Local Rearrangements of Chromophores. In Figure 10, the RMS of each atom in the imidazole plane are compared with the corresponding crystallographic estimates. We notice that although the MD data are lower than experiment they reproduce the overall difference in mobility between the M and L sides, the latter being the most rigid.

We have also evaluated the stability of the spacial arrangement of the cofactors by calculating the distances between their centers of mass, the latter were computed excluding all the atoms of the hydrophobic chains. Figure 11 shows that the simulation reproduces very well the crystallographic geometry of the

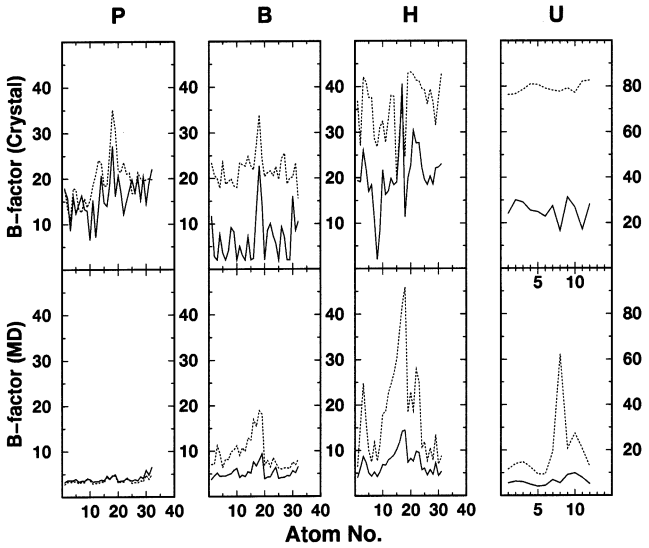

Figure 10. Atomic RMS fluctuations for heavy atoms of the chromophores obtained from MD simulation are converted into *B* factors and compared to the crystallographic values. Only *B* factors of in-plane atoms are shown. Solid lines are results for the chromophores on the L side, and dotted lines are the results for the M side.

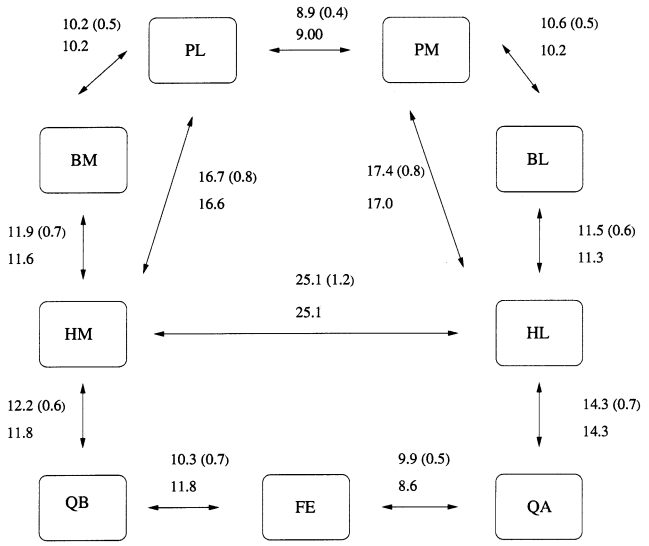

Figure 11. Simulation averaged center of mass distances between cofactors in the RC protein are compared with crystallographic results. Only atoms in the imidazole plane were used to calculate chromophores centers of mass. Values on the top are from simulation and include statistical error in bracket, and X-ray data are on the bottom.

chromophores, with deviations of only a few tenths of an angstrom. Larger deviations, more than 1 Å, are found for distances involving the M-side quinone and the iron ion which are in the region of the RC with the highest crystallographic uncertainties.

Although a small X_{rms} deviation, 1.3 Å, is computed when the simulation is averaged and the X-ray structures of chromophores are superimposed, in the region of the acetyl groups substantial rearrangements are found for P. In particular, our simulation predicts the acetyl group in the imidazole plane of P_M, whereas the X-ray structure of Ermler et al. places it out of this plane. The acetyl oxygens in our MD simulation relaxed very quickly in the imidazole plane with some changes in the minimum distances between the special pair and the two accessory's, see data in Table 3. It must be pointed out that the position and the orientation of this acetyl groups are controversial. In more recent crystallographic structure determinations[36] of mutants of the RC from *Rb. sphaeroides*, Michel and co-workers located the same acetyl group in the imidazol plane with the oxygen pointing toward the other methyl group of the same ring where the acetyl group is attached. Differently, in a series of X-ray structures of the RC from *Rb. sphaeroides*, Feher and co-workers places this group in the imidazol plane, but with a different orientation, the oxygen now pointing to Mg of P_L. This orientation is favored by dielectric continuum calculations[37] which, quite puzzlingly, can account for experimental midpoint potentials for P only for this structure.

TABLE 3: Averaged Minimum Distances on the Last 2.4 ns of Simulation between and the Accessory's Compared with Data from the X-ray Structure[a]

molecules	atom contact	⟨distances⟩	X-ray
$P_M \rightarrow P_L$	C2A−C5	5.12 ± 0.2	5.34
	O(I)−C5	4.80 ± 0.3	5.23
$P_L \rightarrow B_L$	C9−C14	6.20 ± 0.2	5.98
$P_L \rightarrow B_M$	C2A−C5	5.35 ± 0.2	5.04
	O(I)−C5	5.74 ± 0.3	3.92
$P_M \rightarrow B_M$	C9−C14	6.41 ± 0.2	6.14

[a] We used the labels as in ref 43: C2A−O(I) is the acetyl group, C5 is the carbon at the base of ring III not belonging to ring V, C9 is the keto carbon, and C14 is the carbon of ring II bound to the methine bridge between rings II and III.

Only an accurate molecular modeling of the acetyl group in bacteriochlorophylls and bacteriopheophytins, and the calculation of the potential of mean force for the torsional angle involved in the acetyl group isomerization could help clarify this controversy.

The minimum distances between chromophores for both sides were also calculated. These distances are directly related to the electronic coupling between the chromophores. It is well-known that the electronic coupling is proportional to $\exp(-br)$, where r is the distance in Å and $b = 1.47$ Å^{-1}.[38] Thus, changes of a few tenths of Å in distances between chromophores might change the electronic coupling by nearly an order of magnitude. In the calculation of the minimum distances we did not consider the hyperconjugated saturated groups such as methyls. As reported in ref 38, at present there is still no agreement whether these groups can contribute to the electronic coupling in RC.

In Figure 12 the B−H (top) and P−B (bottom) minimum distances are reported. We first notice that the former shows much larger fluctuations than the latter. In particular, on the M side the B−H minimum distance undergoes large jumps of 3 Å at the time. Additionally, P−B distances on both sides show much smaller oscillations with the distance on the M side being consistently 0.4 Å smaller than that on the L side.

For the P−B minimum distances, the closest contacts are between the acetyl groups of the P and the region between ring III and the methine bridge connecting rings II and III of the accessory B's. The different orientations of the acetyl groups in the two monomers of P gives different contacts with the accessory B's: On the L side, the acetyl oxygen is the closest to B, whereas on the M side, the acetyl carbon is the nearest to B. The 0.4 Å difference between the two sides gives a small asymmetry in the coupling factor—with $b = 1.47$, the coupling factor along L is double that along M.

Given that the imidazol rings of B and H are almost perpendicular on both sides, the acetyl groups of B is pointing toward the accessory B. Thus, on both sides the closest contacts is between the H acetyl oxygen and a large region of the B. On the accessory B's the atoms making contact are from ring I and IV including the magnesium. Although on the L side the contacts with H involve, for 90% of the time, the two nitrogens and the

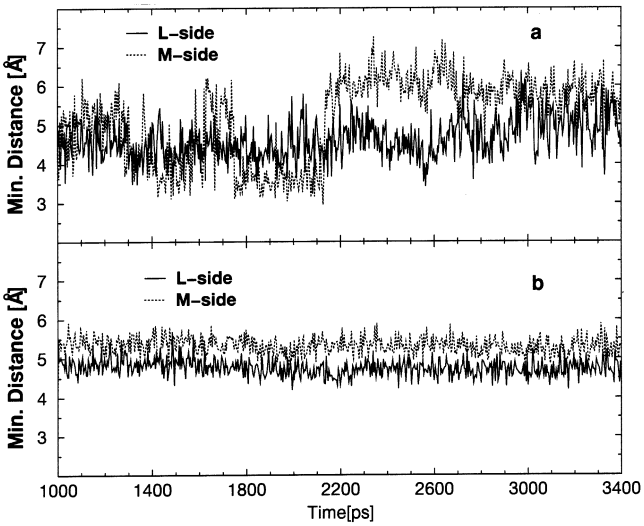

Figure 12. Minimum distances between couples of chromophores along the L (solid line) and M (dotted line) branch. See text for explanation. On panel a are shown distances between accessory B and H on both sides. Panel b shows instead distances between the special pair and B.

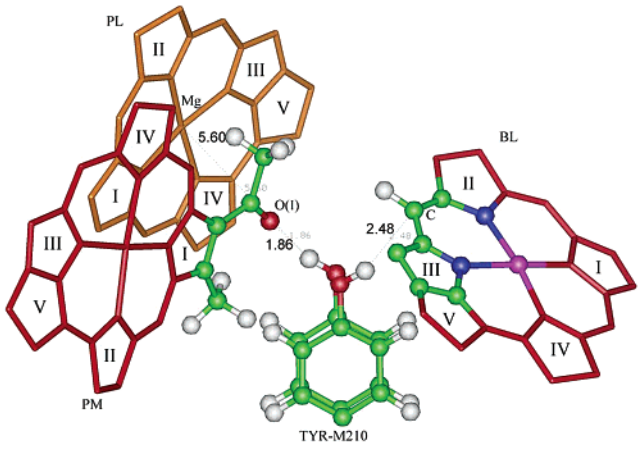

Figure 13. Position of the Tyr-M210 for the two possible orientations of the O−H group. The special pair P and the accessory bacteriochlorophyll B are shown. Atoms at less than 5 Å from the O−H group are represented as balls and sticks.

magnesium, on the M side, the corresponding atoms are only sustaining contacts for about 60% of the time. This is probably due to the larger RMS fluctuations of the H_M and B_M with respect to H_L and B_L, as shown in Figure 10.

2. Orientation of Tyr M210. Because electrostatic interactions have the major effects on static and dynamic of electron transfer, we have examined the relative orientation of Tyr M210, a polar residue, with the capability of making hydrogen bonds, with respect to P_M. During our simulation, M210 is found in two states, depicted in Figure 13, obtained by a 180° rotation along the C−OH bond. Although in the first orientation the hydrogen points toward B_L not binding to any atom in particular, in the second, a hydrogen bond is formed with the acetyl oxygen of P_M. In the former, the transfer of the electron to B_L should be favored given the positive charge of the polar tyrosine hydrogen. However, our simulation indicates that this is not the most probable state, occurring only in 2076 configurations out of 9600. On a previous simulation work on the *Bl. viridis* RC, Parson and co-workers[39] sampled only conformations with the tyrosine O−H bond oriented toward the accessory B_L.

The orientation of the Tyr-M210 is clearly influenced by the atomic charges of chromophores which in our case were derived by high level quantum mechanics calculations. In particular, the orientation of the O−H group is influenced by the negative charge of the methine carbon connecting ring I to II, given a C···H−O distance of 2.5 Å on average. Thus, differences with other investigations[39] might reflect differences in atomic charges. It should also be mentioned that in recent QM/MM investigation[40,41] at the semiempirical level, the position of the Tyr M210 is neither in the direction of B_L nor bound to the acetyl oxygen. As reported in refs 40 and 41, during geometry relaxation, the acetyl group rotated 180° pointing to the magnesium on the L side of P. In another investigation,[42] we find that a relatively small charge perturbation on P and B_L (between −0.2 and −0.4 e^- transferred from P to B_L) already favors the orientation of the tyrosine toward B_L.

IV. Conclusion

This paper has reported on an MD simulation of a RC protein of *Rb. sphaeroides* in a water and detergent solution. The latter component, LDAO a nonionic amphiphile, is used to protect the transmembrane helices of the RC and provides a micelle-like structure to cover the RC hydrophobic regions. The simulated system realistically mimics RC protein solutions, known to be photoactive, and has been used by us to investigate from first principle the primary electron transfer from the excited P* state to H_L.[14] The focus of this first paper has been instead to study the structure and stability of this hydrated molecular complex.

In sum, we find that the LDAO micelle-like structure provides an effective hydrophobic environment which stabilize the RC protein compared with our previous study.[12] For the length of our simulation, 3.4 ns, the overall protein deviation from its X-ray structure remains below 1.75 Å for backbone atoms. Moreover, the computed averaged residue mean square displacements closely reproduce the X-ray results estimated by the B factors. The micelle-like environment surrounding the RC's transmembrane helices is a dynamic and flexible structure, and we observe lateral diffusion for the LDAO molecules much larger than those of the protein but smaller than those of water.

More related to the functionality of this RC protein, we find that the cofactors form a rigid structure for the whole length of the simulation, their atomic RMS on average is smaller than for other protein substructures, and preserve relative distances from each other in good agreement with X-ray. More interestingly, we pinpoint an isomerization of the tyr M210 which is directly coupled with the primary electron transfer. Moreover, in relation with the branch functionality of the RC, we observe that the computed minimum distances between the chromophores on the L and M side have different dynamic behaviors and are smaller on average for transitions on the L side. In particular, the B_M-H_M distance has larger oscillations than that between B_L and H_L. This finding might have some bearing on the electron-transfer asymmetry of the primary event.

Acknowledgment. The work of one of us (M.C.) was supported by an individual Marie Curie grant, Contract No. ERB4001GT974823, held at CECAM/ENS-Lyon, France.

References and Notes

(1) Zhong, Q.; Jiang, Q.; Moore, P.; Newns, D.; Klein, M. *Biophys. J.* **1998**, *74*, 3.

(2) Tieleman, D.; Sansom, M. *Biophys. J.* **1998**, *74*, 2786.

(3) Bond, P.; Faraldo-Gomez, J.; Sansom, M. *Biophys. J.* **2002**, *83*, 763.

(4) Holzapfel, W.; Finkele, U.; Kaiser, W.; Oesterhelt, D.; Scheer, H.; Stiltz, H. U.; Zinth, W. *Chem. Phys. Lett.* **1989**, *160*, 1.

(5) Du, M.; Rosenthal, S. J.; Xie, X.; DiMagno, T. J.; Schmidt, M.; Hanson, D. K.; Schiffer, M.; Norris, J. R.; Fleming, G. R. *Proc. Natl. Acad. Sci. U. S. A.***1992**, *89*, 8517.
(6) Deisenhofer, J.; Epp, O.; Miki, K.; Huber, R.; Michel, H. *J. Mol. Biol.* **1984**, *180*, 385.
(7) Chang, C.; Tiede, D.; Tang, J.; Smith, U.; Norris, J.; Schiffer, M. *FEBS Lett.* **1986,** *205*, 82.
(8) Treutlein, H.; Schulten, K.; Deisenhofer, J.; Michel, H.; Brunger, A.; Karplus, M. In *The photosynthetic bacterial reaction center: Structure and dynamics*; Breton, J., Vermeglio, A., Eds.; Plenum Press: London, 1988; p 139.
(9) Treutlein, H.; Schulten, K.; Deisenhofer, J.; Michel, H.; Brunger, A.; Karplus, M. *Proc. Natl. Acad. Sci. U.S.A.* **1992**, *89*, 75.
(10) Marchi, M.; Gehlen, J.; Chandler, D.; Newton, M. *J. Am. Chem. Soc.* **1993**, *115*, 4178.
(11) Warshel, A.; Parson, W. W. *Quart. Rev. Biophys.* **2001**, *34*, 563.
(12) Souaille, M.; Marchi, M. *J. Am. Chem. Soc.* **1997**, *119*, 3948.
(13) Roth, M.; Lewit-Bentley, A.; Michel, H.; Deisenhofer, J.; Huber, R.; Oesterhelt, D. *Science* **1989**, *340*, 659.
(14) Ceccarelli, M.; Marchi, M. 2002, submitted for publication.
(15) Ermler, U.; Fritzsch, G.; Buchanan, S.; Michel, H. *Structure* **1994**, *2*, 925.
(16) Frolov, D.; Gall, A.; Lutz, M.; Robert, R. *J. Phys. Chem. A* **2002**, *106*, 3605.
(17) Sardet,C.; Tardieu, A.; Luzzati, V. *J. Mol. Biol.* **1976**, *105*, 383.
(18) Hummer, G.; Pratt, L.; Garcia, A. *J. Phys. Chem.* **1996**, *100*, 1206.
(19) Lynden-Bel, R.; Rasaiah, J. *J. Chem. Phys.* **1997**, *107*, 1981.
(20) Ceccarelli, M.; Procacci, P.; Marchi, M. 9th Int. Workshop on Computational Materials Science; Elsevier Science: Amsterdam, 2001; Vol. 20, pp 318−324.
(21) Ceccarelli, M.; Procacci, P.; Marchi, M. *J. Comput. Chem.* **2002**, *24*, 129.
(22) Procacci, P.; Paci, E.; Darden, T.; March, M. *J. Comput. Chem.* **1996**, *18*, 1848.
(23) Procacci, P.; Darden, T.; Marchi, M.; *J. Phys. Chem* **1996**, *100*, 10464.
(24) Marchi, M.; Procacci, P. *J. Chem. Phys.* **1999**, *108*, 5194.
(25) Darden, T.; York, D.; Pederse, L. *J. Chem. Phys.* **1993**, *98*, 10089.
(26) Essman, U.; Pederse, L. Berkowit, M. L.; Darden, T.; Lee, H.; Pedersen, L. G. *J. Chem. Phys.* **1995**, *103*, 8577.
(27) Andersen, H. C. *J. Chem. Phys.* **1980**, *72*, 2384.
(28) Nose, S. *Mol. Phys.* **1984**, *5*, 255.
(29) Tuckerman, M. E.; Berne, B.; Martyna, G. *J. Chem. Phys.* **1990**, *97*, 1992.
(30) Ryckaert, J. P.; Ciccotti, G.; Berendsen, H. J. C. *J. Comput. Phys.* **1977**, *23*, 327.
(31) Andersen, H. *J. Comput. Phys.* **1983**, *5*, 24.
(32) Parrinello, M.; Rahman, A. *J. Appl. Phys.* **1981**, *52*, 7182.
(33) Small, D. *The Physical Chemistry of Lipids*; Plenum Press: New York, 1986).
(34) MacKerell, A., Jr. *J. Phys. Chem.* **1995**, *99*, 1846.
(35) Venable, R.; Zhang, Y.; Hardy, B.; Pastor, R. *Science* **1993**, *26*, 223.
(36) Kuglstatter, A.; Ermler, U.; Michel, H.; Baciou, L.; Fritzsch, G. *Biochemistry* **2001**, *40*, 4253.
(37) Muegge, I.; Apostolaki, J.; Ermler, U.; Fritzsch, G.; Lubitz, W.; Knapp, E. *Biochemistry* **1996**, *35*, 5, 8359.
(38) Kolbasov, D.; Scherz, A. *J. Phys. Chem B* **2000**, *104*, 1802.
(39) Alden, R. G.; Parson, W. W.; Chu, Z. T.; Warshe, A. *J. Phys. Chem.* **1996**, *100*, 16761.
(40) Hutter, M.; Hughes, J.; Reimers, J.; Hus, N. *Phys. Chem B* **1999**, *103*, 4906.
(41) Hutter, M.; Hughes, J.; Reimers, J.; Hus, N. *Am. Chem. Soc.* **2001**, *123*, 8550.
(42) Sterpone, F.; Ceccarelli, M.; Marchi, M. in preparation.
(43) Ceccarelli, M.; Lutz, M.; Marchi, M. *J. Am. Chem. Soc.* **2000**, *122*, 3532.